Measurement of the $\beta\beta$ Decay Half-Life of ^{130}Te with the NEMO-3 Detector

R. Arnold,[1] C. Augier,[2] J. Baker,[3,*] A. S. Barabash,[4] A. Basharina-Freshville,[5] S. Blondel,[2] M. Bongrand,[2]
G. Broudin-Bay,[6,7] V. Brudanin,[8] A. J. Caffrey,[3] A. Chapon,[9] E. Chauveau,[10] D. Durand,[9] V. Egorov,[8] R. Flack,[5]
X. Garrido,[2] J. Grozier,[5] B. Guillon,[9] Ph. Hubert,[6,7] C. Hugon,[6,7] C. M. Jackson,[10] S. Jullian,[2] M. Kauer,[5] A. Klimenko,[8]
O. Kochetov,[8] S. I. Konovalov,[4] V. Kovalenko,[6,7,8] D. Lalanne,[2] T. Lamhamdi,[11] K. Lang,[12] Z. Liptak,[12] G. Lutter,[6,7]
F. Mamedov,[13] Ch. Marquet,[6,7] J. Martin-Albo,[14] F. Mauger,[9] J. Mott,[5] A. Nachab,[6,7] I. Nemchenok,[8] C. H. Nguyen,[6,7,15]
F. Nova,[12] P. Novella,[14] H. Ohsumi,[16] R. B. Pahlka,[12] F. Perrot,[6,7] F. Piquemal,[6,7] J. L. Reyss,[17] B. Richards,[5] J. S. Ricol,[6,7]
R. Saakyan,[5] X. Sarazin,[2] L. Simard,[2] F. Šimkovic,[19] Yu. Shitov,[8,18] A. Smolnikov,[8] S. Söldner-Rembold,[10] I. Štekl,[13]
J. Suhonen,[20] C. S. Sutton,[21] G. Szklarz,[2] J. Thomas,[5] V. Timkin,[8] S. Torre,[5] V. I. Tretyak,[1,8] V. Umatov,[4] L. Vála,[13]
I. Vanyushin,[4] V. Vasiliev,[5] V. Vorobel,[22] Ts. Vylov,[8,*] and A. Zukauskas[22]

(NEMO-3 Collaboration)

[1]*IPHC-DRS, Université Louis Pasteur, CNRS, F-67037 Strasbourg, France*
[2]*LAL, Université Paris-Sud 11, CNRS/IN2P3, Orsay, France*
[3]*INL, Idaho National Laboratory, Idaho Falls, Idaho 83415, USA*
[4]*ITEP, Institute of Theoretical and Experimental Physics, 117259 Moscow, Russia*
[5]*University College London, London WC1E 6BT, United Kingdom*
[6]*Université de Bordeaux, CENBG, UMR 5797, F-33175 Gradignan, France*
[7]*CNRS/IN2P3, CENBG, UMR 5797, F-33175 Gradignan, France*
[8]*JINR, Joint Institute for Nuclear Research, 141980 Dubna, Russia*
[9]*LPC, ENSICAEN, Université de Caen, Caen, France*
[10]*University of Manchester, Manchester M13 9PL, United Kingdom*
[11]*USMBA, Université Sidi Mohamed Ben Abdellah, 30000 Fes, Morocco*
[12]*University of Texas at Austin, Austin, Texas 78712-0264, USA*
[13]*IEAP, Czech Technical University in Prague, CZ-12800 Prague, Czech Republic*
[14]*IFIC, CSIC-Universidad de Valencia, Valencia, Spain*
[15]*Hanoi University of Science, Hanoi, Vietnam*
[16]*Saga University, Saga 840-8502, Japan*
[17]*LSCE, CNRS, F-91190 Gif-sur-Yvette, France*
[18]*Imperial College London, London SW7 2AZ, United Kingdom*
[19]*FMFI, Comenius University, SK-842 48 Bratislava, Slovakia*
[20]*Jyväskylä University, 40351 Jyväskylä, Finland*
[21]*MHC, Mount Holyoke College, South Hadley, Massachusetts 01075, USA*
[22]*Charles University in Prague, Faculty of Mathematics and Physics, CZ-12116 Prague, Czech Republic*

We report results from the NEMO-3 experiment based on an exposure of 1275 days with 661 g of ^{130}Te in the form of enriched and natural tellurium foils. The $\beta\beta$ decay rate of ^{130}Te is found to be greater than zero with a significance of 7.7 standard deviations and the half-life is measured to be $T_{1/2}^{2\nu} = [7.0 \pm 0.9(\text{stat}) \pm 1.1(\text{syst})] \times 10^{20}$ yr. This represents the most precise measurement of this half-life yet published and the first real-time observation of this decay.

The first evidence of $\beta\beta$ decay ($2\nu\beta\beta$) appeared in 1950 through the observation of ^{130}Xe from the decay of ^{130}Te in rock samples [1]. This result was met with scepticism for the ensuing 15 years until the results of a number of other geochemical experiments began to confirm the observation. There was, however, significant disagreement between two distinct sets of these measurements that was not immediately resolved. Several groups measured a long half-life of $\approx 2.7 \times 10^{21}$ yr [2,3] while others obtained a significantly shorter half-life of $\approx 0.8 \times 10^{21}$ yr [4–7].

One hypothesis to explain the difference is based on the observation that shorter half-lives were measured in rock of relatively young age ($\sim 10^7$–10^8 yr), while the longer half-lives were measured in relatively old rock ($\sim 10^9$ yr) [2,4]. It has even been suggested that there is a time dependence in the value of the weak interaction coupling constant [8]. Recent papers [9] attempt to explain the long-held discrepancy between these measurements as being caused by catastrophic xenon loss in the older samples. To date, the only direct evidence for the ^{130}Te $2\nu\beta\beta$

process comes from the MIBETA experiment, which reported a half-life of $[6.1 \pm 1.4(\text{stat})^{+2.9}_{-3.5}(\text{syst})] \times 10^{20}$ yr [10] by comparing different crystals isotopically enriched in ^{130}Te and ^{128}Te, assuming that any difference in rate was due to $2\nu\beta\beta$ events (^{128}Te has a much longer $2\nu\beta\beta$ half-life). However, a systematic uncertainty of about 50% rendered this result somewhat inconclusive. In this Letter, we present the first direct, high-precision measurement of $2\nu\beta\beta$ decay of ^{130}Te with the NEMO-3 detector. In addition, a search for neutrinoless $\beta\beta$ decay ($0\nu\beta\beta$) and for the decay with Majoron emission ($0\nu\chi^0\beta\beta$) is reported.

The NEMO-3 detector is located in the Modane Underground Laboratory. The detector [11] contains almost 9 kg of seven different $\beta\beta$ isotopes in the form of thin foils. It provides direct detection of electrons from the $\beta\beta$ decay by the use of a tracking device based on open Geiger drift cells and a calorimeter made of plastic scintillator blocks coupled to low-radioactive photomultipliers (PMTs). For 1 MeV electrons the timing resolution is 250 ps and the energy resolution (full width at half maximum) is about 15%. A magnetic field surrounding the detector provides identification of electrons by the curvature of their tracks. In addition to the electron and photon identification through tracking and calorimetry, the calorimeter measures the energy and the arrival time of these particles while the tracking chamber can measure the time of delayed tracks associated with the initial event for up to 700 μs. The calorimeter energy scale is calibrated approximately once per month using a ^{207}Bi source providing conversion electrons of 482 and 976 keV (K-lines). Stability of the calorimeter response is surveyed twice a day by a laser system. The data presented in this Letter correspond to 1275 days of data taking between October 2004 and December 2009. Two different foils are used in the analysis: a Te foil, enriched at a level of $89.4 \pm 0.5\%$ corresponding to 454 g of ^{130}Te, and a natural Te foil which contains 33.8% ^{130}Te, corresponding to 207 g of ^{130}Te.

When searching for rare processes, the background estimation is paramount as it will limit the final sensitivity of the experiment. An exhaustive program of work has been carried out to measure the very large number of sources of background present in the NEMO-3 detector. The method of the background measurement and its validation with a highly radiopure Cu foil is described in [12]. There are three categories of background: the external background, originating from radioactivity outside the tracking chamber; the tracking volume background, which includes radon in the tracking gas and the drift cell wire contamination; and the internal background due to radioactive impurities inside the source foils whose dominant isotopes are ^{40}K, ^{234m}Pa, ^{210}Bi, ^{214}Bi, and ^{208}Tl. The different background contributions are estimated by measuring independent event topologies, both for enriched and natural Te.

The external background originates from components outside the tracking volume. PMTs are the main contributors since they have glass and electronic components that,

though at a very low level, contain traces of ^{214}Bi, ^{208}Tl and ^{40}K. The external background is measured with γ-ray Compton scattering in the scintillators, either producing an electron that crosses the tracking chamber or depositing energy in one scintillator, followed by an electron emitted from the source to another scintillator. The reliability of the external background model is illustrated by the energy distributions of the one-electron crossing events in Figs. 1(a) and 1(b).

The source foil activities in ^{234m}Pa, ^{40}K, and ^{210}Bi are determined with single-electron events coming from the foil. The energy distribution of the observed events and the result of the fit of the different components of the background are presented in Figs. 1(c) and 1(d). The good agreement between the data and the fit demonstrates the reliability of the internal background model. The foil activity in ^{214}Bi is measured using events with a single electron accompanied by a delayed α-particle track. This topology is a signature of the β decay of ^{214}Bi to ^{214}Po followed by α decay of ^{214}Po to ^{210}Pb. The foil activity in ^{208}Tl is measured with events that contain one electron and either two or three photons emitted from the foil. The results of measurements of the internal contamination by ^{214}Bi and ^{208}Tl are reported in [12]. The measured foil activities are summarized in Table I.

The background from single β decay in the tracking volume is of importance if the decay occurs near the foil. The main source of this background is due to daughters of radon: ^{214}Pb, ^{214}Bi, and ^{210}Bi. The radon activity in the tracking chamber is measured using $e\alpha$ events as for the
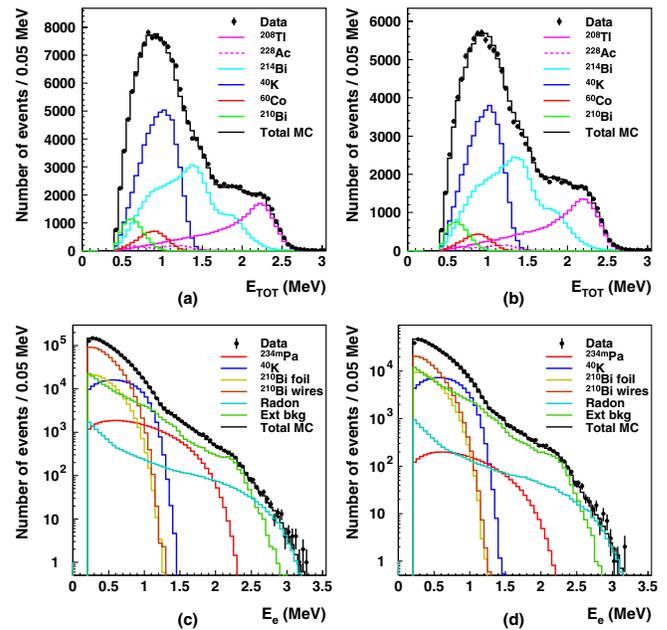

FIG. 1 (color online). Energy sum distribution for crossing-electron events for (a) ^{130}Te and (b) ^{nat}Te (b); Energy distribution of electron events coming from the source foil for (c) ^{130}Te and (d) ^{nat}Te. Dots correspond to the data and histograms to the fit of the background model.

TABLE I. Background contaminations measured in the Te source foils (in mBq).

Impurity	^{130}Te	^{nat}Te
^{208}Tl	0.17 ± 0.04	0.24 ± 0.04
^{214}Bi	0.29 ± 0.05	0.25 ± 0.12
^{234m}Pa	2.49 ± 0.05	0.73 ± 0.04
^{210}Bi	19.9 ± 0.4	18.4 ± 0.3
^{40}K	14.7 ± 0.2	12.3 ± 0.2

measurement of internal ^{214}Bi background. The distribution of these events is measured as a function of the location in the tracking volume. For the data presented here, the mean ^{222}Rn activity in the whole gas volume is 209 ± 2 mBq. Unlike the preceding radon daughters, ^{210}Pb has a long half-life of about 22 years. It is therefore not in equilibrium with ^{222}Rn in the tracking volume and most ^{210}Pb was deposited during the construction of the detector. ^{210}Bi produced in β decay of ^{210}Pb contributes to the low-energy background below 1 MeV. The ^{210}Pb deposition on drift cell wires, measured by detecting electrons from ^{210}Bi β decay, was found to be vary significantly in different sectors [12]. In contrast to ^{222}Rn the concentration of ^{220}Rn in NEMO-3 is very small and its contribution to the total background in the ^{130}Te sectors is less than 1%.

The measured activities are used to estimate the background contribution in the two-electron channel with a Monte Carlo (MC) simulation. Signal and background MC events are generated using a GEANT-based simulation [13] of the detector with the initial kinematics given by the event generator DECAY0 [14].

The two-electron events are selected with the following requirements. Two tracks of a length greater that 50 cm with curvature corresponding to a negative charge are reconstructed. Both tracks originate from a common vertex in the foil and terminate in isolated scintillators with a single energy deposit greater than 0.2 MeV. The time-of-flight information is consistent with the hypothesis that two electrons were emitted from the same point on the source foil. No photon or delayed α track is detected in the event. These selection criteria lead to a $2\nu\beta\beta$ detection efficiency of 3.5% for enriched ^{130}Te and 2.8% for ^{nat}Te, where the difference is mainly due to the source foil thickness. Several factors contribute to this low efficiency, but the most important are the geometrical acceptance of the detector, the effect of the energy threshold, and the tracking algorithm inefficiencies.

We measure the ^{130}Te half-life with data from the enriched Te source foil by performing a likelihood fit to the binned energy sum distribution in the interval [0.9–2] MeV. This interval is chosen using the MC simulation to maximize the signal significance. It reduces the $2\nu\beta\beta$ efficiency by a factor of 0.7. The result of the fit is presented in Figs. 2(a), 2(c), and 2(e). Using the MC simulation the number of background events in the interval [0.9–2] MeV is estimated to be 363 ± 25 events, of which 141 events are associated with the external background, 179 with the
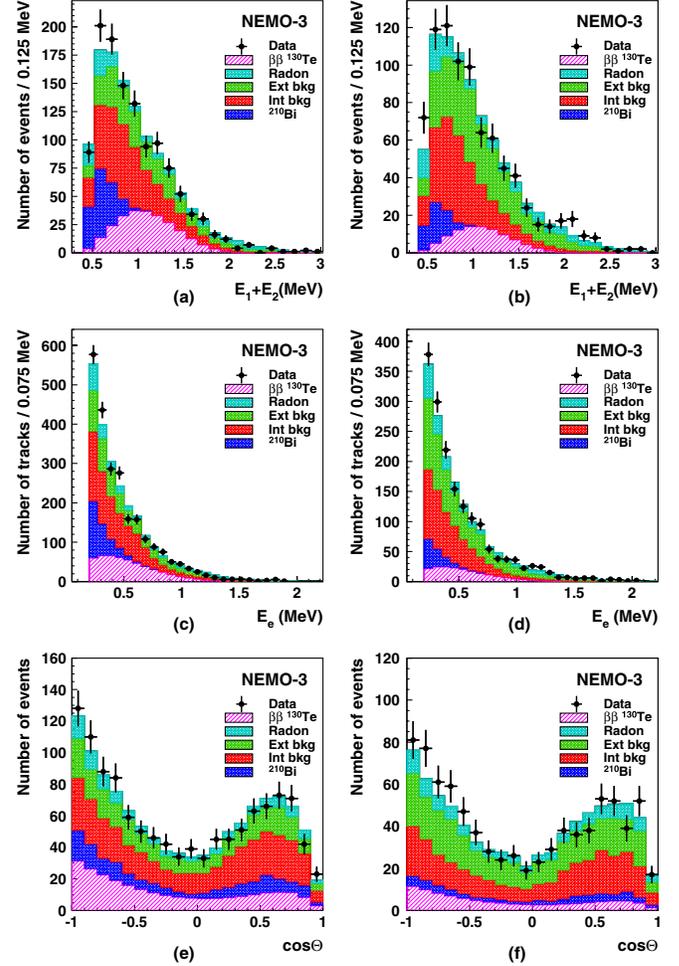

FIG. 2 (color online). (a),(b) Distribution of the sum of the electron energies; (c),(d) individual electron energy; and (e), (f) cosine of the angle between the electron tracks for two-electron events selected from the two Te foils: (a),(c),(e) enriched in ^{130}Te and (b),(d),(f) natural Te.

internal background, and 43 with radon induced background. The number of events in excess of the background in the interval [0.9–2] MeV is determined to be

$$n(2\nu\beta\beta) = 178 \pm 23, \qquad (1)$$

with a signal significance of 7.7 standard deviations and a signal-to-background ratio of $S/B = 0.5$. This corresponds to a ^{130}Te half-life of

$$T_{1/2}^{2\nu} = (7.0 \pm 0.9) \times 10^{20} \text{ yr.} \qquad (2)$$

The main systematic uncertainty on the measured ^{130}Te half-life is associated with the background estimation and is due to the small signal-to-background ratio. The uncertainty on the number of expected background events has been obtained by applying the largest variations of the component activities in the background model. The corresponding uncertainty on the ^{130}Te half-life is 14%. Another systematic uncertainty is associated with the two-electron detection efficiency in NEMO-3 which is found to be

correct within an accuracy of 5%. This uncertainty is determined with a calibrated ^{207}Bi source and a dedicated ^{90}Sr source which decays to ^{90}Y, a pure β emitter of $Q_\beta = 2.28$ MeV. Finally, the source foil thickness and the GEANT model of electron energy losses in dense thin media contribute a systematic uncertainty of 4% which is estimated by comparing signals from metallic and composite ^{100}Mo source foils [15]. The total systematic uncertainty of 15% is obtained by adding the individual contributions in quadrature.

The measurement of the $2\nu\beta\beta$ half-life is verified using the natural Te foil. The energy and angular distributions of the two-electron events of the natural Te data are presented in Figs. 2(b), 2(d), and 2(f) and are compared with the expected MC distribution using the measured half-life $T_{1/2}^{2\nu} = 7.0 \times 10^{20}$ yr and the background model of the natural Te foil. There are 65 ± 8 $\beta\beta$ events and 316 ± 28 background events expected in the electron energy sum interval [0.9–2] MeV. The total number of 381 ± 29 expected events is in good agreement with the 377 observed events.

The ^{130}Te data [Fig. 2(a)] are also used to set a limit on the $0\nu\beta\beta$ and $0\nu\chi^0\beta\beta$ processes with the modified frequentist analysis [16]. The method uses the full information of the binned energy sum distribution for signal and background, as well as the statistical and systematic uncertainties and their correlations as described in [17].

The total efficiency to detect $0\nu\beta\beta$ decay of ^{130}Te is estimated to be (13.9 ± 0.7)% yielding a limit of

$$T_{1/2}^{0\nu} > 1.3 \times 10^{23} \text{ yr (90\% C.L.)}, \qquad (3)$$

which is an order of magnitude less stringent than the limit obtained by the CUORICINO experiment [18] based on 11 kg of ^{130}Te.

The detection efficiency for the decay with ordinary (spectral index $n = 1$) Majoron emission (see discussion in [19] and references therein) is (9.6 ± 0.5)% and the limit is determined to be

$$T_{1/2}^{0\nu\chi_0} > 1.6 \times 10^{22} \text{ yr (90\% C.L.)}, \qquad (4)$$

which is a factor of 7 more stringent than the previous best limit from MIBETA [10]. The corresponding limit on the coupling constant of the Majoron to the neutrino is $g_{ee} < (0.6–1.6) \times 10^{-4}$ (using nuclear matrix elements from [20–24]) and is comparable with the best present limits.

In summary, the $2\nu\beta\beta$ decay ^{130}Te half-life measured with the NEMO-3 detector is

$$T_{1/2}^{2\nu} = [7.0 \pm 0.9(\text{stat}) \pm 1.1(\text{syst})] \times 10^{20} \text{ yr.} \qquad (5)$$

With this result, the corresponding nuclear matrix element can be extracted according to

$$(T_{1/2}^{2\nu})^{-1} = G^{2\nu}|M^{2\nu}|^2, \qquad (6)$$

where $G^{2\nu} = 4.8 \times 10^{-18}$ yr^{-1} (for $g_A = 1.254$) is the known phase space factor [25], which yields the result $M^{2\nu} = 0.017 \pm 0.002$ (scaled by the electron mass). This

value for $M^{2\nu}$ may be used to fix the g_{pp} parameter of the quasiparticle random-phase approximation model, which corresponds to the strength of the nucleon-nucleon interaction inside the nucleus. It has been suggested that this will improve the $M^{0\nu}$ calculations [20,21,26].

The NEMO-3 result for the ^{130}Te half-life is consistent with the geological measurements made in younger rock samples and is the most precise measurement of this isotope half-life to date.

*Deceased.

[1] M. G. Inghram and J. H. Reynolds, Phys. Rev. **78**, 822 (1950).

[2] T. Kirsten *et al.*, in: *Nuclear Beta Decays and the Neutrino* edited by T. Kotani, H. Ejiri, and E. Takasugi (World Scientific, Singapore, 1986), p. 81.

[3] T. Bernatowicz *et al.*, Phys. Rev. C **47**, 806 (1993).

[4] O. K. Manuel, in *Nuclear Beta Decays and the Neutrino*, edited by T. Kotani, H. Ejiri, and E. Takasugi (World Scientic, Singapore, 1986), p. 71.

[5] W. J. Lin *et al.*, Nucl. Phys. **A481**, 477 (1988).

[6] N. Takaoka and K. Ogata, Z. Naturforsch. A **21**, 84 (1966).

[7] N. Takaoka, Y. Motomura, and K. Nagano, Phys. Rev. C **53**, 1557 (1996).

[8] A. S. Barabash, JETP Lett. **68**, 1 (1998); Eur. Phys. J. A **8**, 137 (2000); Astrophys. Space Sci. **283**, 607 (2003).

[9] A. P. Meshik *et al.*, Nucl. Phys. **A809**, 275 (2008); H. V. Thomas *et al.*, Phys. Rev. C **78**, 054606 (2008).

[10] C. Arnaboldi *et al.*, Phys. Lett. B **557**, 167 (2003).

[11] R. Arnold *et al.*, Nucl. Instrum. Methods Phys. Res., Sect. A **536**, 79 (2005).

[12] R. Arnold *et al.*, Nucl. Instrum. Methods Phys. Res., Sect. A **606**, 449 (2009).

[13] R. Brun *et al.*, CERN Program Library W 5013, 1984.

[14] O. A. Ponkratenko *et al.*, Phys. At. Nucl. **63**, 1282 (2000).

[15] R. Arnold *et al.*, Nucl. Phys. **A781**, 209 (2007).

[16] T. Junk, Nucl. Instrum. Methods Phys. Res., Sect. A **434**, 435 (1999).

[17] R. Argyriades *et al.*, Phys. Rev. C **80**, 032501(R) (2009).

[18] C. Arnaboldi *et al.*, Phys. Rev. C **78**, 035502 (2008).

[19] R. Arnold *et al.*, Nucl. Phys. **A765**, 483 (2006).

[20] F. Simkovic *et al.*, Phys. Rev. C **77**, 045503 (2008).

[21] M. Kortelainen and J. Suhonen, Phys. Rev. C **76**, 024315 (2007).

[22] E. Caurier *et al.*, Phys. Rev. Lett. **100**, 052503 (2008).

[23] J. Barea and F. Iachello, Phys. Rev. C **79**, 044301 (2009).

[24] P. K. Rath *et al.*, Phys. Rev. C **82**, 064310 (2010).

[25] J. Suhonen and O. Civitarese, Phys. Rep. **300**, 123 (1998).

[26] V. Rodin *et al.*, Nucl. Phys. **A766**, 107 (2006); **A793**, 213 (2007).